Proc. 31st Int. Workshop on Vertex Detectors (VERTEX2022)
JPS Conf. Proc. **42**, 011006 (2024)
https://doi.org/10.7566/JPSCP.42.011006

Performance of the CMS Silicon Strip Tracker

Suvankar Roy Chowdhury on behalf of the CMS Collaboration

INFN Sezione di Pisa, Italy

E-mail: sroychow@cern.ch

(Received January 17, 2023)

The CMS silicon strip tracker, consisting of 15148 silicon modules with a 200 m^2 active area, has been successfully taking data in LHC Run 1 and Run 2. After the second long shutdown period from the end of 2018 the detector resumed operations in the fall of 2021, first with cosmic rays, followed by collisions at 900 GeV, before LHC started regular Run 3 operation at a centre-of-mass energy of 13.6 TeV in summer 2022. The tracker will be operational till the end of LHC Run 3, before the HL-LHC upgrade. In this contribution, the performance of the detector during the Run 2 will be summarized. The projections of the detector performance during Run 3 will be discussed, with particular emphasis on the expected changes in detector performance with increasing irradiation. The performance of the detector during the early Run 3 collisions will also be presented.

KEYWORDS: CMS, Silicon Strip tracker...

1. Introduction

The CMS apparatus [1] at the Large Hadron Collider (LHC) is a nearly hermetic multipurpose detector, designed to identify electrons, muons, photons as well as charged and neutral hadrons. The tracking system [1,2] of the CMS experiment is based on silicon sensor technology, using pixels in the inner and micro strips in the outer part. In this report, the performance of the silicon strip tracker (SST) with pp collisions during LHC Run 2 (2015-2018) and early Run 3 (2022) will be discussed.

2. Description of the silicon strip tracker

The SST is instrumented with 15148 silicon modules, having an active area of 200 m^2. One quarter of the SST in r-z view is shown in Fig. 1. It is organized into four sub-partitions. In the barrel region, the modules are organized in four layers of the Tracker Inner Barrel (TIB), and six layers of the Tracker Outer Barrel (TOB). The first two layers of both TIB and TOB are instrumented with **stereo modules**, where two independent modules are mounted back-to-back with their strips aligned at a relative angle of 100 mrad. This stereo angle between the strips enables 3D measurement of particle hits. In the forward region on each side of the barrel, the SST is made up of Tracker Inner Disk (TID) and Tracker Endcap (TEC) sub-detectors. The TID has modules arranged in three disks, each with three rings of modules, whereas in the TEC, the modules are arranged in nine disks with 4-7 rings of modules. Rings 1 and 2 of TID, and rings 1,2, and 5 of TEC are also instrumented with stereo modules. The silicon sensors of SST are of p-in-n type, with p^+ implants in the n-type silicon bulk. The sensors have two different thicknesses - either 320 μm in TIB, TID and the inner rings of TEC, and 500 μm in TOB and the outer rings of TEC. The silicon sensors of the SST are read out by the APV25 front-end chip [3].

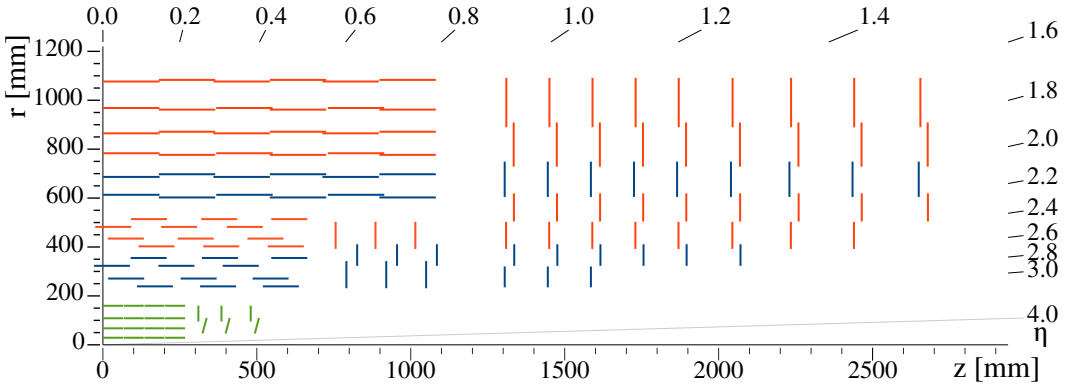

Fig. 1. Sketch of one quarter of the CMS tracking system in r-z view. The pixel detector is shown in green. Single-sided and double-sided (stereo) strip modules are depicted as red and blue segments, respectively.

3. Performance of the silicon strip tracker

In this section, the performance of the SST during LHC collision period Run 2 (2015-2018) and early Run 3 (2022) will be discussed.

3.1 Cluster charge

Local reconstruction of the SST data starts by joining adjacent strips which have a charge above a threshold to form a cluster. To reconstruct trajectories of charged particles, the clusters from both the pixel and SST are used. Tracks are reconstructed in multiple iterations. Clusters belonging to a track are called **on-track clusters**. Details of the track reconstruction can be found in Ref. [4]. Since the cluster charge is affected by radiation, the strip charge signal is corrected by a constant gain factor in order to guarantee the stability of the most probable value (MPV) of the cluster charge over time. The gain factor is derived by normalizing the MPV to the same value corresponding to that for a minimum ionizing particle. The calibration is performed every about 10 fb^{-1} . The corrected cluster charge as a function of the delivered integrated luminosity during Run 2 is shown in Fig. 2, which shows clear stability over time. Large fluctuations in the cluster charge in the first 20 fb^{-1} of 2016 data are caused by the saturation of the pre-amplifier of the APV25 chip (Section 5) [5].

3.2 Signal to noise ratio

The signal-to-noise ratio (S/N) for on-track clusters is one of the most important observable of the SST. The S/N is crucial for the separation of signals generated by charged particles and fluctuations coming from detector noise. Examples of S/N distributions for TIB is shown in Fig. 3 for a run taken in 2018 (left) and a run taken in 2022 (right). A fit is performed to the distribution using a Landau function convoluted with a Gaussian function. The extracted MPV from the fit is quoted as the S/N. The values of the S/N for representative runs taken during Run 2 and 2022 are reported in Table 3.2. Measurements are performed per sub-detector and split by the sensor thickness in the TEC. The signal over noise ratio is dropping with the integrated fluence. The S/N is also high at the beginning of Run 3. The evolution of the S/N for pp data taking during Run 2 is shown in Fig. 4. Projecting the trend to the end of Run 3 (~500 fb^{-1}), the S/N will be about 12 (18) for the thin (thick) sensors, which will still allow the SST to deliver high quality data for physics analyses.

3.3 APV25 pre-amplifier saturation effects

During 2015 and early part of the 2016 data taking period, a lowering of SST S/N and loss of hits on tracks were observed. This behaviour was caused by saturation effects in the pre-amplifier of

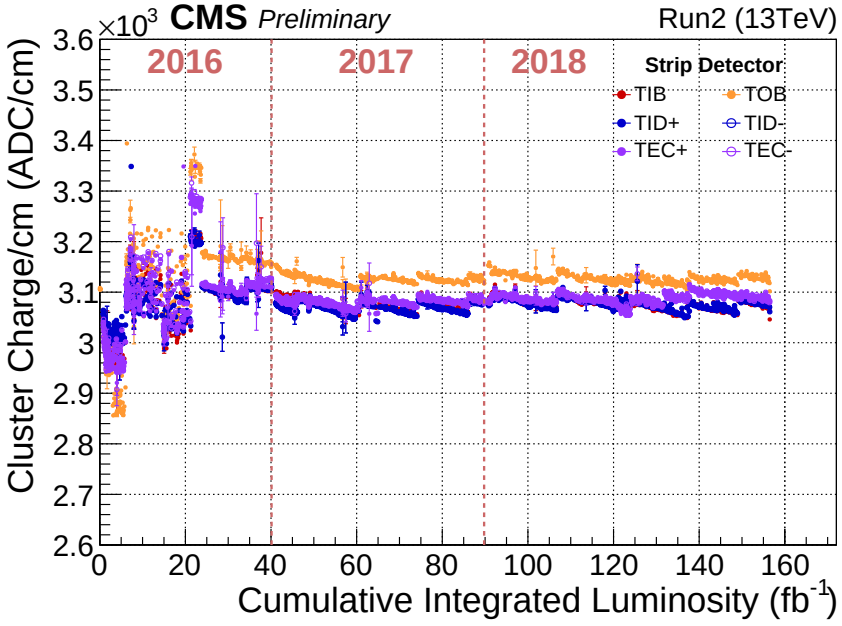

Fig. 2. Cluster charge normalized to the traversed silicon length after offline calibration for each partition of the SST as a function of the delivered LHC integrated luminosity. Each point represents a single run.

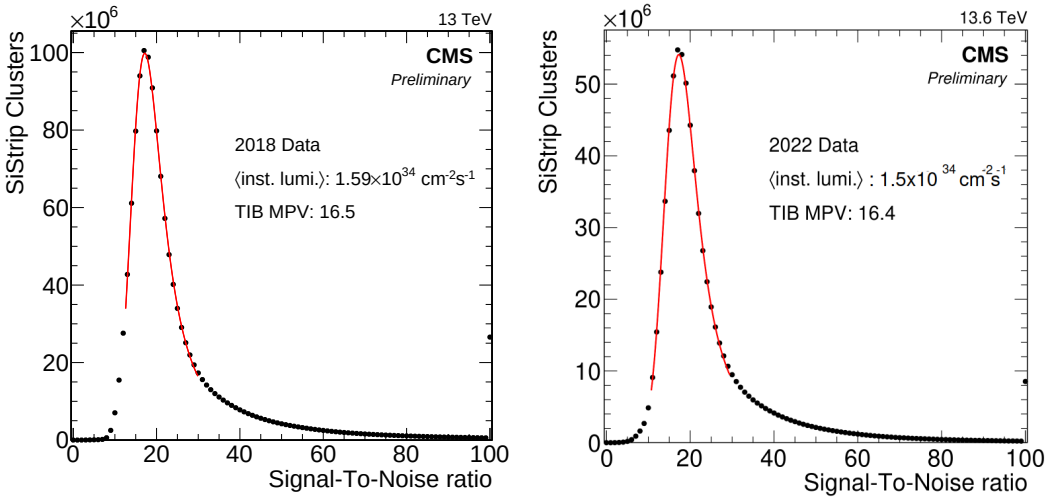

Fig. 3. Distributions of the signal-to-noise ratio in the TIB for a representative run taken in 2018 (left) and 2022 (right), respectively.

the APV25 readout chip. The drain speed of the pre-amplifier of the APV25 chip was affected by a lowering of the operating temperature, leading to a very slow discharge of the amplifier with a decay constant $O(15\,\mu s)$ [5]. The effect had a strong instantaneous luminosity dependence and affected the first $20\,fb^{-1}$ of 2016 data. The drain speed was changed in August 2016 to mitigate this effect. In order to improve the description of 2016 data in the period affected by the APV25 saturation issue, the simulation of the SST includes a dedicated description of the saturation effect, details of which can be found in Ref. [5]. Figure 5 shows the distribution of the on-track cluster charge in the first layers of

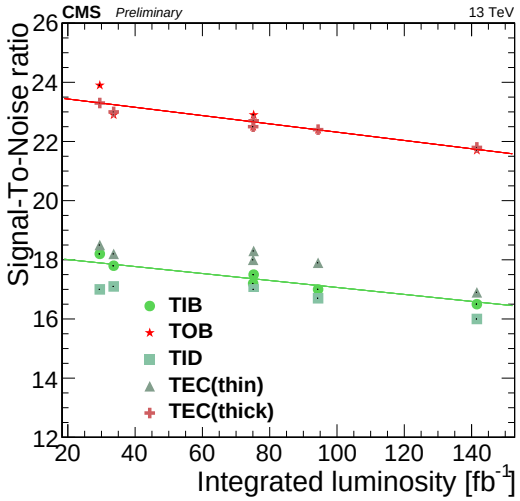

Fig. 4. The signal-over-noise ratio measured in pp collision during Run 2 as a function of the integrated luminosity.

Table I. The signal-to-noise ratio for all sub-detectors of the SST for each data taking year.

Year	TIB	TOB	TID	TEC (thin)	TEC (thick)
2016	17.2	22.5	16.7	18.0	22.5
2017	17.5	22.9	17.0	18.3	22.7
2018	16.5	22.1	16.0	16.9	21.8
2022	16.4	21.0	16.4	17.4	21.5

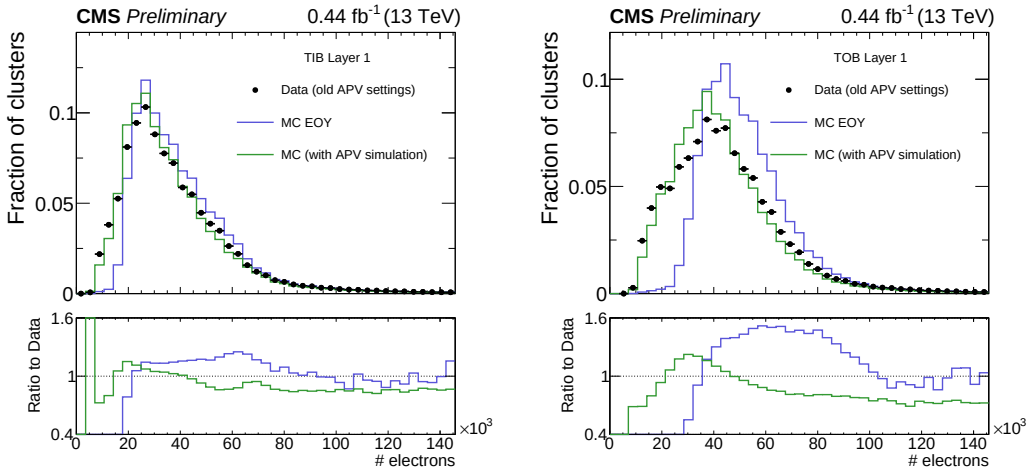

Fig. 5. **Left**: Distribution of cluster charge for the first layer of TIB. **Right**: Distribution of cluster charge for the first layer of TOB.

the TIB (left), and TOB (right). The simulated sample of minimum bias events including a description of the APV dynamic gain, "MC (with APV dynamic gain)", gives an improved description of the data

compared to the sample without this description, "MC EOY".

3.4 Fraction of bad readout channels

It is crucial to constantly monitor the fraction of bad readout channels during operation, in order to mitigate the impact on track reconstruction. During data taking, the bad components are evaluated automatically by a Prompt Calibration loop algorithm [6] identifying very noisy channels based on the median channel occupancy. Along with that, the fraction of channels excluded from data taking due to various thermal, electrical issues are also marked as bad. The fraction of bad readout channels of the SST as a function of integrated luminosity delivered during Run 2 is shown in Fig. 6 (left). The larger variations of about 2% observed in the TID- sub-detector are caused by faulty power groups excluded from readout during 2016 and at the beginning of 2017. TID being a smaller sub-detector is more susceptible to variations even for a low number of additionally lost modules. The difference of a few percents observed between TID+ and TID- sub-detectors is caused by a problematic cooling loop present in TID-. Figure 6 (right) shows the time evolution of the fraction of bad channels for 2022 pp collisions, split by sub-detector. The drop in bad module fraction between August and September 2022 in the endcaps is due to a recovery of a cooling loop in the TEC+. The disproportionate impact of a change in end-caps bad component fraction on the detector average is caused by the fact that this sub-detector comprises more than 40% of all the modules of the silicon strip detector. In both the trends, the fraction of the bad components is very stable. Since the SST design has redundancy in tracking layers, the exclusion of these bad channels does not degrade track reconstruction efficiency significantly.

3.5 Hit efficiency

The hit efficiency is defined as the ratio of the number of measured hits to the number of expected hits belonging to a track. The high signal-to-noise ratio results in excellent in-time hit reconstruction efficiencies for all SST partitions. Hit efficiency is evaluated for all layers and disks of SST, and regularly monitored during operations. It is computed using tracks from the iterative tracking passing the 'highPurity' selection [4]. Modules which are marked bad for offline reconstruction are not used in the measurement of the hit efficiency. The hit efficiency of all TIB layers as a function of instantaneous luminosity and number of pile-up interactions, is shown in Fig. 8 (top). Data from the long LHC fill 6714 of 14 hours taken in 2018 have been used. The same is shown for all TOB layers in Fig. 8 (bottom). From the trends, it can be seen that the hit efficiency is above 98% even for the highest pile-up and instantaneous luminosity. The average hit efficiency in all SST layers and disks, for a run taken in 2018 is shown in Fig. 7. The mean number of pile-up interactions in the run was 31 and the peak instantaneous luminosity was 1.11×10^{34} cm^{-2}s^{-1}. The average efficiency is found to be at or above 99% in all the layers or disks of the SST.

3.6 Hit resolution

The spatial resolution of reconstructed hit positions is computed by using hits in overlapping modules of the same layer ("pair method") [7, 11]. This method reduces the effects of multiple scattering and the bias coming from misalignment. Figure 9 (left) shows the hit resolution for strips with different pitch and for different cluster widths (expressed in units of number of strips), and compared to the expected resolution for binary readout (pitch/$\sqrt{12}$). For all cluster widths, the measured hit resolution is seen to be better than the binary resolution showing the benefit of charge sharing due to the analogue readout. The expected scaling with the strip pitch is also seen. The hit resolution as a function of the expected cluster width is shown in Fig. 9 (right), for all layers of the TIB. As the cluster width and hence the amount of charge sharing between neighbouring strips increases, the spatial resolution improves.

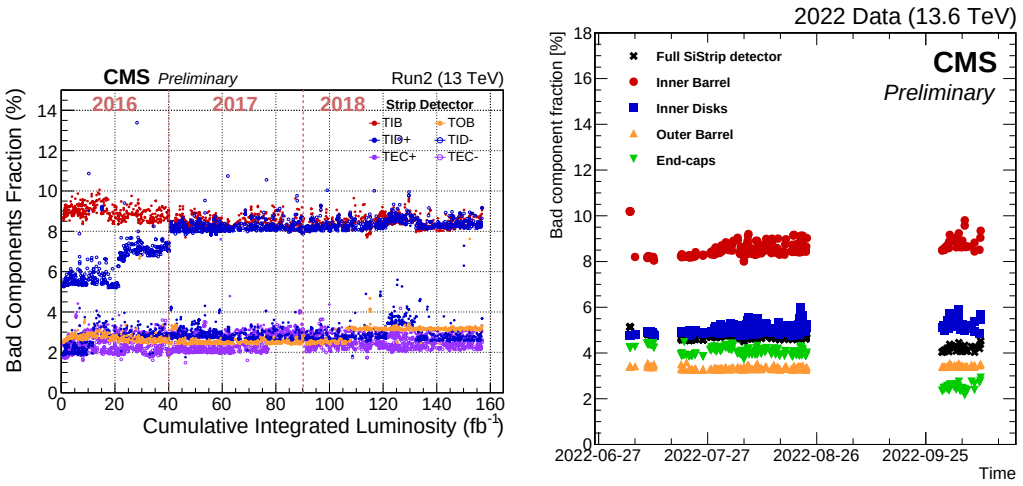

Fig. 6. **Left**: The fraction of bad readout channels the SST as a function of integrated luminosity delivered during Run 2. **Right**: Time evolution of the global fraction of readout channels flagged as bad for offline reconstruction for early Run 3 pp collisions.

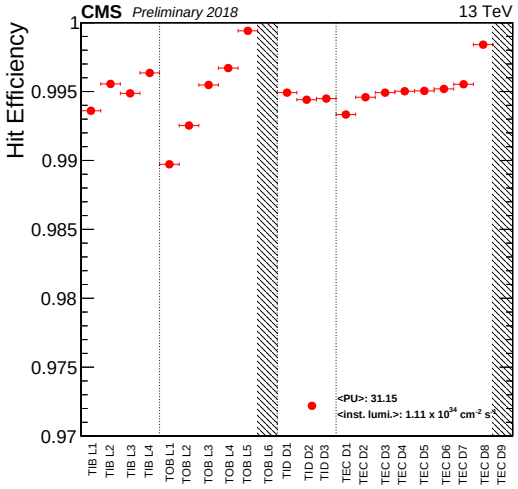

Fig. 7. Efficiency for all SST layers and disks during a run in 2018. The two Grey bands correspond to the outermost layers where the efficiency cannot be measured.

4. Effects of radiation

Operation at the high energy pp collisions exposes the SST to high levels of radiation affecting not only the silicon sensors, but also associated module components. The effect of accumulated radiation damage in the sensors is assessed by measuring the leakage current and the full depletion voltage (V_{FD}). The leakage current and sensor temperature are measured by Detector Control Units (DCU) [2] on the individual modules and compared to simulation. The simulation is based on the Hamburg model [9] and takes into account the fluence and temperature of the sensors. The temperature evolution is taken into account in the simulation by using measurements from the detector itself. The evolution of the leakage current per cubic centimeter scaled to 0°C, in TIB layers as a

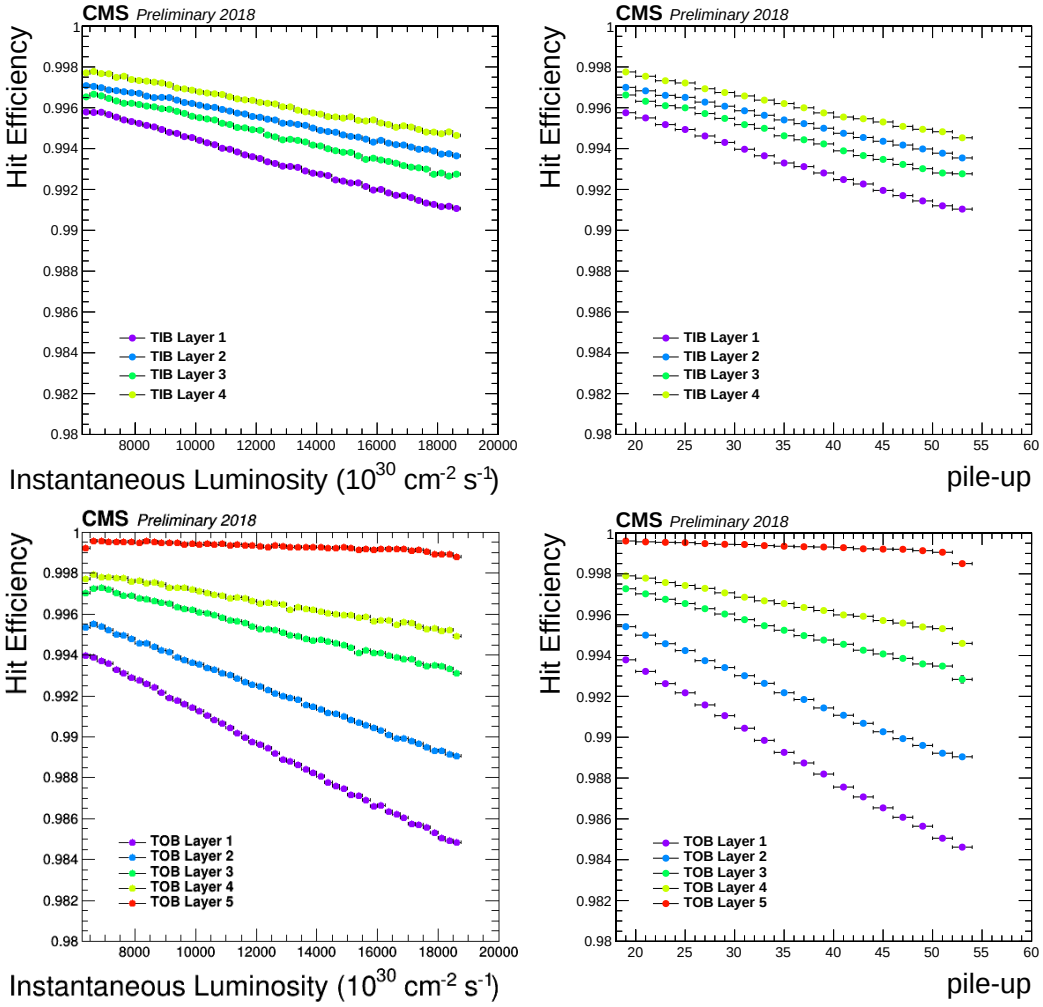

Fig. 8. **Top**: Hit efficiency in all layers of the TIB as a function of instantaneous luminosity (left) and pile-up (right). **Bottom**: Hit efficiency in all layers of the TOB as a function of instantaneous luminosity (left) and pile-up (right).

function of the integrated luminosity is shown in Fig. 10 along with comparisons to estimates from simulation. The current in a layer is the average for all sensors (for which data is available), after scaling the current to its equivalent at 0°C [10]. The data are extracted when the LHC beam status was stable. While the differences between simulation and measurement as well as the slight difference between Run 1 and 2 require further investigations, it is estimated to be within the uncertainties of the FLUKA simulations as well as within the uncertainties on the simulation model parameters.

The evolution of leakage current is used in projections of the detector performance with increased irradiation. Figure 11 shows the geometrical representation of the modules in various sub-detectors expected to experience thermal runaway at the end of Run 3 (assuming a total integrated luminosity 400 fb^{-1}), with the coolant temperature set to -20°C (top) and -25°C (bottom). Setting the coolant temperature to −25°C reduces the number of modules with thermal runaway by half. Studies are ongoing to understand the performance of tracking in these scenarios.

Regular bias voltage scans are performed during data taking either on the full detector (twice per year) or on a selected group of modules (once per month) to measure V_{FD} . The V_{FD} is determined by analyzing curves of the evolution of the cluster width, which depends on the depleted volume, as

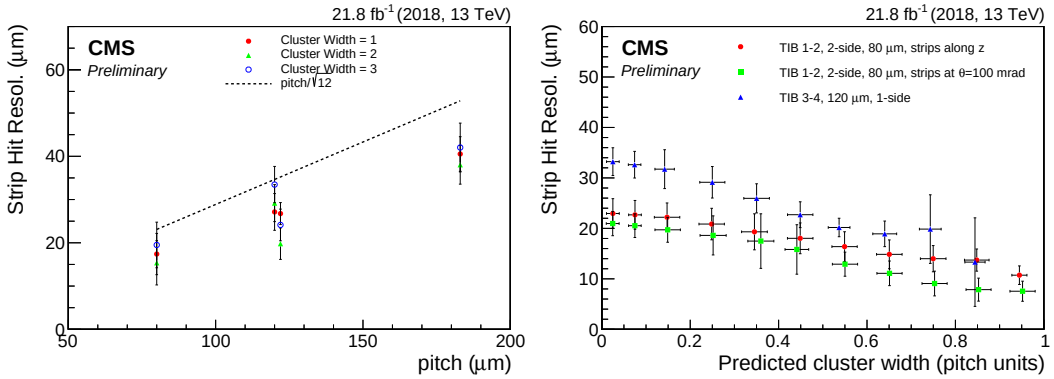

Fig. 9. **Left**: Strip hit resolution in different types of overlapping sensors and for different cluster widths. The expected resolution for binary readout (pitch/$\sqrt{12}$) is also shown for comparison. **Right**: Strip hit resolution for modules in TIB as a function of predicted cluster width.

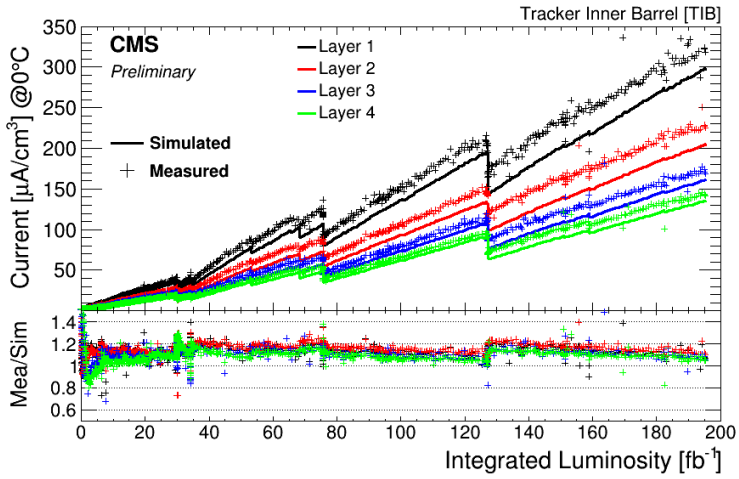

Fig. 10. The leakage current per cubic centimeter normalized to to 0°Cas a function of integrated luminosity for TIB layers.

a function of the bias voltage. The saturation point is extracted from linear fits of the two regimes of the curve as illustrated in the Fig. 12 (left). Their crossing point gives the position of the full depletion voltage estimation. The evolution of the full depletion voltage for one TIB Layer 1 sensor as a function of the integrated luminosity and fluence until the end of LHC Run 2 is show in Fig. 12 (right). The break occurring at an integrated luminosity close to 30 fb^{-1} in the curves is due to the long shut down period between Run 1 and 2. The opening of the CMS detector and cooling plant maintenance resulted in extended periods during which the silicon detector was not cooled as well as it would have been desirable from the radiation damage point of view. This led to a visible accumulation of reverse annealing. Small increases due to annealing are visible at 75 fb^{-1} and 130 fb^{-1} which correspond to winter shutdown periods. In the hashed area, the estimates of the depletion voltage from data has large uncertainties. In this case, the full depletion voltage is set to the value of the first voltage setting with clusters reconstructed. It is therefore not possible to deduce from the data, the exact position of the inversion point. Data as well as the model prediction, suggest that the TIB Layer 1 reached the inversion point at the end of LHC Run 2.

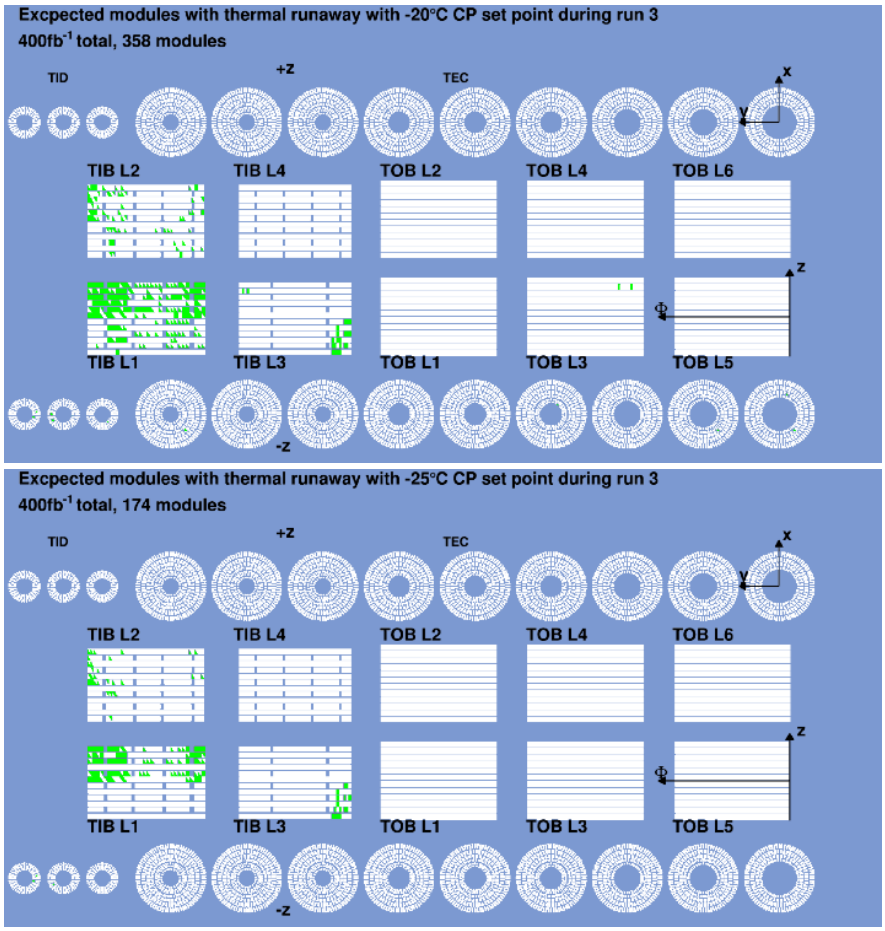

Fig. 11. The leakage current per cubic centimeter as a function of integrated luminosity for TIB layers with the coolant temperature set to -20 °C (top) and -25 °C (bottom).

5. Conclusion

The CMS SST is collecting data successfully at the LHC after for more than ten years of operation. The detector had stable performance throughout Run 2 and in early Run 3 (2022). High signal-to-noise ration and stability of the cluster charge have been observed. The hit efficiency in all sub- detectors is above 98%, even under high pile-up conditions. The number of active channels in the SST is above 95%, and is stable over time. Radiation effects on the sensor are estimated by monitoring the V_{FD} and leakage current periodically. The performance of the SST at the startup of Run 3 data taking is excellent. Projections show that the SST can perform efficiently till the end of Run 3.

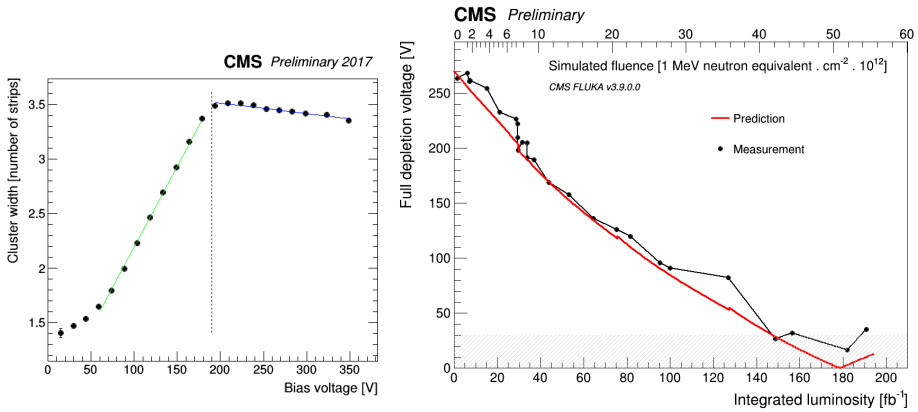

Fig. 12. **Left**: The leakage current per cubic centimeter as a function of integrated luminosity for TIB layers. **Right**: Evolution of the V_{FD} for one TIB Layer 1 sensor as a function of the integrated luminosity and fluence until the end of LHC Run 2.

References

[1] The CMS Collaboration, The CMS experiment at the CERN LHC, JINST **3**, S08004 (2008).
[2] The CMS Collaboration, The CMS tracker: addendum to the Technical Design Report, CERN-LHCC-2000-016., CMS TDR 5 Addendum 1, (2000).
[3] L. L. Jones, M. J. French, Q. R. Morrissey, A. Neviani, M. Raymond, G. Hall, P. Moreira, and G. Cervelli, The APV25 deep submicron readont chip for CMS detectors, doi:10.5170/CERN-1999-009.162, (1999).
[4] The CMS Collaboration, Description and performance of track and primary-vertex reconstruction with the CMS tracker, JINST **9** (2014) P10009.
[5] The CMS Collaboration, Simulation of the Silicon Strip Tracker pre-amplifier in early 2016 data, CERN-CMS-DP-2020-045, (2020).
[6] G. Cerminara, B. van Besien, and on behalf of the CMS Collaboration, Automated workflows for critical time-dependent calibrations at the CMS experiment, Journal of Physics: Conference Series **664**,072009 (2015) .
[7] CMS Tracker Collaboration,Stand-alone cosmic muon reconstruction before installation of the CMS silicon strip tracker, JINST **4** P05004 (2009).
[8] The CMS Collaboration, Silicon Strip Tracker Performance results 2018, CERN-CMS-DP-2018-052 (2018).
[9] M. Moll, Radiation damage in silicon particle detectors: Microscopic defects and macroscopic properties, DESY-THESIS-1999-040, Hamburg U. (1999).
[10] A. Chilingarov, Temperature dependence of the current generated in Si bulk, JINST **8** P10003 (2013).
[11] CMS Tracker Collaboration,Silicon Strip Tracker Performance results 2018, CERN-CMS-DP-2018-052.